Calculation of Vibrational Spectra of Linear Tetrapyrroles. 4. Methine Bridge C−H Out-of-Plane Modes

Maria Andrea Mroginski,* Daniel Horacio Murgida, and Peter Hildebrandt

Technische Universität Berlin, Institut für Chemie, Max-Volmer-Laboratorium, Sekr. PC 14, Strasse des 17. Juni 135, D-10623 Berlin, Germany

Received: May 22, 2006; In Final Form: July 14, 2006

Quantum chemical force fields obtained by density functional theory (DFT) calculations systematically overestimate the frequencies of normal modes including ethylenic C−H out-of-plane (HOOP) coordinates. Compensation of this deviation requires a specific scaling factor for this type of coordinate that is distinctly lower than those applicable to out-of-plane coordinates in general. Such a specific scaling factor (0.900) has been optimized for the DFT(B3LYP) level of theory on the basis of vibrational analyses of training molecules including the HOOP coordinate. Thus, the root-mean-square deviation for the calculated frequencies of these modes is reduced from 16 to 8 cm^{-1}. Although Raman intensities are yet not reproduced in a satisfactory manner, implementation of the HOOP scaling factor into the set of global scaling factors determined previously (Magdo et al. *J. Phys. Chem. A* **1999**, *103*, 289−303) allows for a substantially improved reproduction of the experimental (resonance) Raman spectra of test molecules including linear methine-bridged tetrapyrroles. A very good agreement between calculated and experimental spectra is noted for the phycocyanobilin dimethylester dimer as well as for the protein-bound phycocyanobilin in the antenna pigment α-CPC. However, for the phycocyanobilin chromophore in the P_r state of the plant photoreceptor phytochrome phyA, considerable deviations remain in the spectral range between 800 and 500 cm^{-1}, which are attributed to the effect of specific protein−chromophore interactions. The influence of the protein environment is not considered in the present calculations that refer to the molecule in vacuo.

Introduction

Calculations of the vibrational frequencies by quantum chemical ab initio methods are being increasingly used for the analysis of vibrational spectra. With increasing size of the molecules, the number of modes observed in the experimental IR and Raman spectra grows strongly such that, particularly for molecules of low symmetry, an unambiguous spectra interpretation is not possible on the basis of empirical approaches and intuitive arguments. In this respect, quantum mechanically calculated spectra become an indispensable tool for the vibrational assignment, which is a prerequisite for the determination of structural parameters from the spectra. For molecules including more than 25 atoms, quantum mechanical calculations are usually restricted to the harmonic approximation which, together with the intrinsic deficiencies of the methods employed, leads to systematic errors of the force fields. These drawbacks can be partially overcome by applying scaling procedures.

Whereas scaling of the calculated frequencies by a single factor already significantly improves the agreement with the experimental frequencies, the scaled quantum mechanics force field (SQMFF) approach developed by Pulay and co-workers provides physically sustained and thus more accurate corrections.[1] In this approach, global scaling factors are introduced to correct the force field itself. Within a specific level of theory, these scaling factors are optimized for a particular type of internal coordinates and, thus, are transferable between different molecules that include the same or chemically similar internal coordinates. Therefore, the scaling factors can be initially determined for molecules for which a complete vibrational assignment is straightforward, i.e., training molecules, and then transferred to the target molecules.

Several sets of global scaling factors have been developed and improved in the past decade affording an agreement of the calculated frequencies with the experimentally determined data of ca. ±10 cm^{-1}.[1,1−3] Extending the scaling procedures to target molecules has provided promising results even for molecules containing more than 60 atoms, and there are no indications for a principle size limit. In view of this generally very good performance, the few striking deviations that have been noted deserve specific attention. For example, it has been found that the force constants for internal coordinates involving the N−H group cannot be consistently corrected by the same scaling factors in the presence and absence of hydrogen bond interactions.[4] With the introduction of specific scaling factors for hydrogen-bonded N−H functions, a substantial improvement of the description of experimental spectra is achieved. This is particularly important for analyzing the spectra of protein cofactors such as linear tetrapyrroles which are usually involved in a network of hydrogen bonds with adjacent amino acid residues. Linear tetrapyrroles such as phytochromobilin, phycocyanobilin, and biliverdin constitute the chromophoric sites in phytochromes, a family of photoreceptors, that have been studied by resonance Raman (RR) spectroscopy.[5−8] SQMFF calculations have been shown to be indispensable for the interpreting the experimental RR spectra. On the basis of the analysis of the spectral region between 1300 and 1700 cm^{-1}, conclusions can be drawn about the configuration, conformation, and protonation state of the tetrapyrroles, and in this way,

* E-mail: andrea.mroginski@tu-berlin.de.

10.1021/jp063128x CCC: $33.50
Published on Web 08/23/2006

valuable information about the molecular functioning of phytochrome has been obtained.

The most striking discrepancies between experimental and calculated spectra refer to the region of the methine bridge C−H out-of-plane (HOOP) modes with frequency deviations of up to 50 cm^{-1}. This failure of the calculations is particularly annoying, since HOOP modes are considered to be sensitive indicators for dihedral distortions for the methine bridges of tetrapyrroles and, more generally, for polyene chains. The present paper is dedicated to overcoming this deficiency by developing an optimized scaling factor for HOOP modes which so far is not included in the set of global scaling factors. The strategy is based on the vibrational analyses of a series of eight test molecules that include the HOOP coordinate. For these molecules, the vibrational spectra are calculated using density functional theory (DFT). By comparing the calculated and experimental spectra, an HOOP scaling factor is optimized and included in the set of transferable scaling factors, which in the subsequent step is employed for the description of the vibrational spectra of test and target molecules that include tetrapyrroles in different configurations and conformations.

Methods

Calculations. DFT calculations with the B3LYP functional[9] and the 6-31G* [10] basis set were carried out as described previously.[3] The force fields were scaled according to

$$(F_{ij})^{\sigma} = \sqrt{\sigma_i}(F_{ij})\sqrt{\sigma_j} \tag{1}$$

where $(F_{ij})^{\sigma}$ and F_{ij} are the respective scaled and unscaled force constants of the internal coordinates *i* and *j*. A previously determined set of global scaling factors σ_i was used together with the scaling factor for the HOOP coordinate, σ_{HOOP}, which is introduced in this work. Optimization of the force field scaling factor for the HOOP coordinate is performed as described by Baker et al.,[11] using a least-squares merit function defined as

$$f(\sigma_{HOOP}) = \sqrt{\Sigma[\nu_i^{exp} - \nu_i^{calc}(\sigma_{HOOP})]^2} \tag{2}$$

where ν_i^{exp} are the experimental frequencies and $\nu_i^{calc}(\sigma_{HOOP})$ are the frequencies calculated on the basis of the scaled force field using σ_{HOOP}. The summation in eq 2 runs over all experimental vibrational frequencies of all molecules of the training set. Minimization of the $f(\sigma_{HOOP})$ is done using a Newton−Raphson optimization algorithm. The gradient and the Hessian matrix can be obtained by differentiating eq 2 with respect to the scaling factor σ_{HOOP}. These quantities are evaluated in each optimization step. Convergence is considered to be achieved when the changes of the σ_{HOOP} scaling factor are smaller than $1 \cdot 10^{-3}$.

Geometry optimization, force constants, as well as dipole moment and the polarizability derivatives calculation were performed using the program package *Gaussian03*.[12] Programs developed in our laboratory were employed for the normal-mode analysis as well as for the evaluation of Raman intensities and the optimization of the force field scaling factor.[3]

The matrix elements of the dipole moment and the polarizability derivatives which determine the IR and Raman intensities were evaluated using the program package *Gaussian03*. For off-resonance excitation, the Raman intensities $I_{Ra,i}$ of a normal mode *i* with frequency ν_i is given by eq 3

$$I_{Ra,i} \propto [45(\alpha')^2 + 7(\gamma')^2]\frac{(\nu_0 - \nu_i)^4}{\nu_i\left[1 - \exp\left(-\frac{h\nu_i}{kT}\right)\right]} \tag{3}$$

where α' and γ' are the derivatives of the mean polarizability α and its anisotropy γ with respect to the normal mode *i*. This equation refers to a setup where the incident light is in the *x*-direction, being linearly polarized in the *z*-direction, and the scattered light is observed in the *y*-direction.

Experimental Methods. RR spectra of PCBE, α-CPC, and phytochrome were measured with 1064-nm excitation as described previously.[13] The preparation of the C-15 deuterated PCB isotopomer and the vibrational analysis of its phytochrome adduct (65-kDa fragment of phyA from oat) will be described in detail elsewhere.

Results and Discussion

Selection of Training and Test Molecules. The hierarchy of the molecules constituting the benchmarks of the project is illustrated in Figure 1. The training molecules serve for the determination of a scaling factor for the ethylenic HOOP internal coordinate, σ_{HOOP}, which then will be added to a set of transferable scaling factors and applied to the test molecules. All the training molecules include at least one ethylenic CH group. In addition, the compounds had to fulfill two criteria. First, only those compounds have been chosen for which accurate structural data are available as a criterion for checking the goodness of the quantum mechanical geometry optimization. Second, the experimental infrared and Raman spectra of the compounds must refer to well-defined states (preferentially monomeric states) and must possess a sufficient quality as a prerequisite for a safe vibrational assignment and thus for the determination of an accurate value for the scaling factor. In this way, we have selected eight different compounds: butadiene, propene, isoprene, pentadiene, 2-methyl-2-butene, styrene, stilbene, and hexamethylpyrromethene (HMPM). Among them butadiene, propene, and HMPM have been used in previous scaling factor optimization procedures.[3,4,11]

The test molecules include 2,4-hexadiene, phycocyanobilin dimethylester (PCBE), and the protein-bound phycocyanobilin (PCB) of the α-subunit of C-phycocyanin of *Mastigocladus laminosus* (α-CPC).[13] Hexadiene is taken as an example of linear conjugated polyenes. Polyenes constitute fundamental building blocks of the chromophoric groups of many relevant biological proteins, such as retinals in rhodopsins or carotenoids in photosynthetic proteins. The vibrational properties of hexadiene have been extensively studied by Mohamed et al.[14] PCBE and the protein-bound PCB are linear tetrapyrroles in two different conformations. For both tetrapyrroles, three-dimensional structure data can either be derived from experimental studies on related compounds or have been determined directly. Both PCBE and PCB in α-CPC may be considered ideal test molecules, since they are closely related to the target molecules, i.e., phytochrome cofactors, which includes tetrapyrrolic chromophores of a priori unknown configuration and conformation.

The crystal structure of α-CPC reveals a protonated PCB chromophore ($PCBH^+$) in an extended *ZZZasa* configuration.[15] Vibrational data of the protein-bound chromophore are available by means of RR spectroscopy.[13] In contrast, PCBE in organic solvents and in the solid state most likely forms dimers via hydrogen bond interactions involving the carbonyl functions and the NH groups of the terminal pyrrolidone and/or pyrrolone rings, as has been previously observed in biliverdin dimethyl-

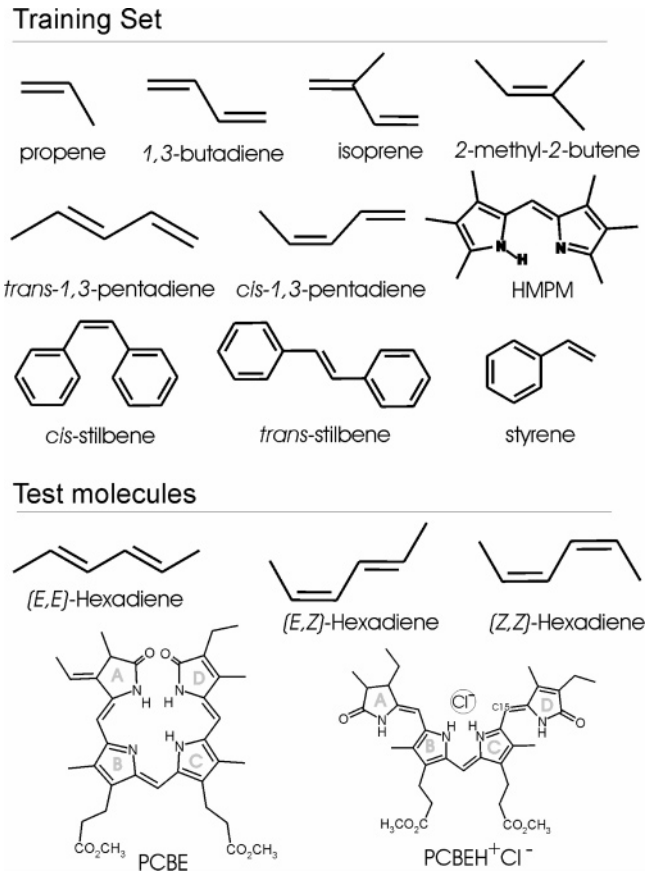

Figure 1. Structural formulas of training and test molecules.

ester crystals.[16] These dimers exhibit a helical structure resulting from two monomeric units with *ZZZsss* conformation and configuration of the methine brigdes.

Geometry Calculations. The geometries of the training and target molecules were optimized at the B3LYP/6-31G* level of theory with tight convergence cutoffs on the forces and the step size. In general, experimental structural data were used for comparison, except for 2-methyl-2-butene and 1,3-pentadiene for which no structural data are available. Optimized geometries are in excellent agreement with experimental values as indicated in Table 1.

Training Molecules. Butadiene and isoprene may exist in two and three different conformations, respectively. According to spectroscopic and thermodynamic data,[17−19] the *s-trans*-butadiene and *s-trans*-isoprene prevails such that calculations of the vibrational spectra were restricted to these conformers. For both compounds, the minimum-energy structures obtained at the B3LYP/6-31G* level of theory are in excellent agreement with the experimental data (Table 1). A comparably good agreement between calculated and experimental structures is also obtained for propene (Table 1).[20]

For 1,3-pentadiene, geometry optimization reveals three stable conformers, the s-cis,trans, the s-trans,trans, and the s-trans,cis isomers. In agreement with microwave spectroscopic studies,[21] the two s-trans species are predicted to be the most stable ones, which therefore were considered for frequency calculations. Among them, the *s-trans*,*cis*-1,3-pentadiene is calculated to be higher in energy by 6.95 kJ/mol than the *s-trans*,*trans*-1,3 pentadiene. The two pentadiene isomers exhibit planar backbone geometries. The trans/cis isomerization of the C═C double bond induces an opening of the inner C−C═C angles by 3° while keeping the C−C and C═C bond lengths unchanged.

The optimized structures of *cis*-stilbene and its *trans*-stilbene exhibit nonplanar structures with the phenyl rings rotated in ca. 2.4° (*trans*-stilbene) and 33.5° (*cis*-stilbene) about the C-phenyl bond. These torsional coordinates are underestimated compared to the experimental values of 3.4−6.8° and 43° for *trans*- and *cis*-stilbene, respectively.[22,23] Furthermore, the calculated bond length alternation at the ethylene bridge is predicted to be less pronounced than the experimental values, corresponding to an overestimation of electronic delocalization and thus a higher degree of conjugation in the DFT calculations. The crystal structure of styrene[24] indicates a small torsion angle between the phenyl ring and the vinyl group of 7.82°, whereas the calculations afford a perfectly planar geometry. Here, a comparable underestimation of the calculated C═C bond length of the vinyl substituent is noted as for stilbene.

Hexamethyl pyrromethene (HMPM) crystallizes in the form of dimers held together by NH···N hydrogen bonds.[4] This structure agrees very well with the geometry of the dimeric species optimized at the B3LYP/6-31G* level of theory. In monomeric HMPM, the calculated geometry remains nearly unchanged compared to the monomeric entities of the dimer. The calculations indicate only a slight (0.002 Å) decrease of the C−C bond length at the methine bridge and a 2.4° opening of the corresponding C−C═C angle upon dimerization (Table 1).

Test Molecules. Three hexadiene structures were taken into account in this work, corresponding to the isomerization states at the C═C double bonds, i.e., (*Z*,*Z*), (*E*,*E*), and (*Z*,*E*). Although for each case six rotational isomers are expected as a combination of trans- (*t*) and cis- (*c*) rotations around the three C−C bonds, only the lowest-energy structures were considered for further force field calculations. Among all possible rotamers, the (*ttt*) conformation turned out to be the most stable one. The DFT calculations predict the lowest-energy structure (*EE*,*ttt*) hexadiene, followed by (*ZE*,*ttt*) and (*ZZ*,*ttt*), which are higher in energy by 1.425 and 3.045 kcal/mol, respectively. The geometry calculated for the (*EE*,*ttt*) isomer coincides with those previously published by Mohamed et al.[14] A slight elongation by 1−4 mÅ of the C−C and C═C bonds as well as the opening of the C−C═C angles (ca. 2−3°) of (*ZZ*,*ttt*) and (*ZE*,*ttt*) isomers indicate an increase of steric interaction compared to (*EE*,*ttt*). Since experimental structural parameters of hexadiene are not available, we compared the B3LYP structures with ab initio MP2/6-311+G* calculations (Table 1, Supporting Information). The differences between the geometries obtained at both levels of theory are small with discrepancies in the C═C/C−C bond lengths and C═C−C bond angles of ≤0.001 Å and ca. 0.6°, respectively. The B3LYP/6-31G* calculations predict slightly more extended backbone structures compared to those obtained with MP2/6-311+G*. The same effect has been observed for pentadiene and 2-methyl-2-butene (Table 1).

Since the crystal structure of the phycocyanobilin dimethyl ester (PCBE) is not available, the starting geometry was built from the crystal structure of the closely related biliverdin dimethyl ester. This tetrapyrrole has a *ZZZsss* conformation and forms hydrogen-bonded dimers via the N−H and C═O groups of the rings A and D, such that we expected the same dimers for PCBE as well. NMR and circular dichroism studies[25] have shown that at least two diastereoisomers of PCBE coexist in solution, an M-helical and a P-helical form. The experimental studies as well as B3LYP calculations for PCBE monomers indicate that the M-helical form is more stable by only 0.1 kcal/mol than the P-form. To find the appropriate dimeric stuctrure of PCBE, we constructed four possible centrosymmetric helical

TABLE 1: Averaged Structural Parameters of the Training Molecules Calculated at the B3LYP/6-31G* Level of Theory[a]

	bond lengths			bond angles
	C−H	C−C	C−C	C−C═C
butadiene[19]	1.091 (1.090)	1.458 (1.463)	1.341 (1.341)	124.3 (123.3)
propene[20]	1.091 (1.090)	1.502 (1.501)	1.333 (1.336)	125.2 (124.3)
isoprene[18]	1.090	1.468 (1.463)	1.340 (1.34)	126.1 (127.3)
2-methyl-2-butene	1.091 [1.091]	1.503 [1.502]	1.342 [1.349]	128.8 [128.2]
cis-1,3 pentadiene	1.090 [1.092]	1.501 [1.501] (C4−C5)	1.346 [1.352] (C3═C4)	127.8 [127.3] (C3═C4−C5)
		1.457 [1.460] (C2−C3)	1.341 [1.349] (C1═C2)	127.1 [126.6] (C2−C3═C4)
				123.8 [122.9] (C1═C2−C3)
trans-1,3 pentadiene	1.091	1.499 [1.499] (C4−C5)	1.343 [1.349] (C3═C4)	125.2 [124.6] (C3═C4−C5)
		1.456 [1.459] (C2−C3)	1.341 [1.348] (C1═C2)	124.3 [123.8] (C2−C3═C4)
				124.6 [124.6] (C1═C2−C3)
cis-stilbene[22]	1.090	1.475 (1.489)	1.350 (1.334)	131.2 (129.5)
trans-stilbene[23]	1.089	1.466 (1.472)	1.349 (1.336)	127.2 (126.0)
styrene[24]	1.090 (0.98)	1.472 (1.474)	1.339 (1.325)	127.7 (126.8)
HMPM[4]	1.087 (0.93)	1.419 (1.411)[b]	1.374 (1.373)[b]	126.6 (128.3)

[a] Experimental values are given in parentheses. Structural parameters calculated at the MP2/6-311+G* level of theory are listed in brackets. [b] Averaged over the two monomeric units.

TABLE 2: Structural Parameters of PCBE-HCl (*ZZZasa*) and PCBE (*ZZZsss*) Calculated with B3LYP/6-31G*

	α-CPC	$PCBH^+Cl^-$ *ZZZasa*	PCBE *ZZZsss*			BVE[27] *sss*	2,3-dihydrobilatriene-abc[26] *ZZZsss*
	exptl	calcd	calcd			exptl	exptl
			monomer	DD-dimer	AA-dimer		
				Bridge AB			
C═C[a]	1.405	1.355	1.366	1.365	1.363	1.351	1.338
C−C[a]	1.423	1.444	1.434	1.436	1.434	1.421	1.466
CCC[b]	133.8	128.9	125.5	125.2	128.9	125.3	124.6
N_ACCC[c]	20.8	−3.1	4.8	2.9	13.8		1.4
$CCCN_B$[c]	133.8	147.4	14.2	10.1	23.9		12.7
				Bridge BC			
C═C[a]	1.411	1.396	1.379	1.379	1.389	1.373	1.368
C−C[a]	1.421	1.397	1.417	1.417	1.405	1.385	1.426
CCC[b]	133.9	133.8	126.6	127.4	127.8	127.3	126.8
N_BCCC[c]	4.3	1.5	4.7	4.2	5.3		4.8
$CCCN_C$[c]	5.3	2.7	3.4	7.9	2.3		8.1
				Bridge CD			
C═C[a]	1.4161	1.441	1.366	1.364	1.363	1.357	1.343
C−C[a]	1.4154	1.360	1.431	1.432	1.438	1.477	1.438
CCC[b]	129.4	127.5	128.9	129.6	126.7	125.4	130.3
N_CCCC[c]	141.1	144.6	13.2	16.0	7.6		16.2
$CCCN_D$[c]	1.1	−2.9	4.9	8.8	1.2		3.3

[b] Bond lengths are given in angstroms. [b] Bond angles are given in degrees. [c] Dihedral angles are given in degrees.

dimers by combining the M-helical monomeric units, each with two possible tautomeric states, i.e., one with a pyrrolic B-ring and the other one with a pyrrolic C-ring. Geometry optimization of these structures at the B3LYP/6-31G* level of theory indicates that the most stable conformation corresponds to a C-pyrrolic tail-to-tail dimer (DD dimer), followed by the B-pyrrolic head-to-head dimer (AA dimer) that is higher in energy by 3.19 kcal/mol. The two remaining conformations, the C-pyrrolic head-to-head and the B-pyrrolic tail-to-tail dimers, are predicted to exhibit energies that are higher by 7.55 and 7.76 kcal/mol, respectively.

In Table 2, the optimized geometries of the two most stable dimeric PCBE conformations are compared with the crystallographic structure of a 2,3-dihydrobilatriene-abc derivative[26] and with biliverdin dimethyl ester.[27] Unlike biliverdin, the 2,3-dihydrobilatriene-abc crystallizes in helical dimers linked by hydrogen bonds between the rings D of the two centrosymmetrically related molecules with acidic protons at the nitrogens of rings A, C, and D. Thus, it constitutes a good reference system for the comparison with the optimized backbone geometry of the C-pyrrolic-PCBE dimer with DD conformation.

The C═C and C−C distances of the methine bridges of both PCBE conformers (AA and DD) agree within ∼0.01−0.03 Å with the values extracted from the two available crystal structures. The calculated C−C═C angles and the corresponding dihedral angles of the methine bridges of the DD dimer are in good agreement with the 2,3-dihydrobilatriene-abc structure with deviations of less than 1° and 6° for the bond angles and dihedral angles, respectively. The C−C═C methine bridge angles of the head-to-head (AA) conformation were compared with the corresponding structural parameters of free biliverdin. The largest deviation is found for the AB methine bridge angle which is overestimated by 3.6°. Dimerization of PCBE has a negligible effect on the C═C and C−C distances of the methine bridges, since the differences between the corresponding bond lengths of the monomer and those of the dimer do not exceed 0.002 Å. The same conclusion holds for the methine bridge angles, which increase by less than 1°. Only slight twists (0.5−4.5°) of the bridges are predicted to occur. Since the structure of free PCBE with DD conformation is predicted to be the most stable one and its geometry is in very good agreement with the crystal

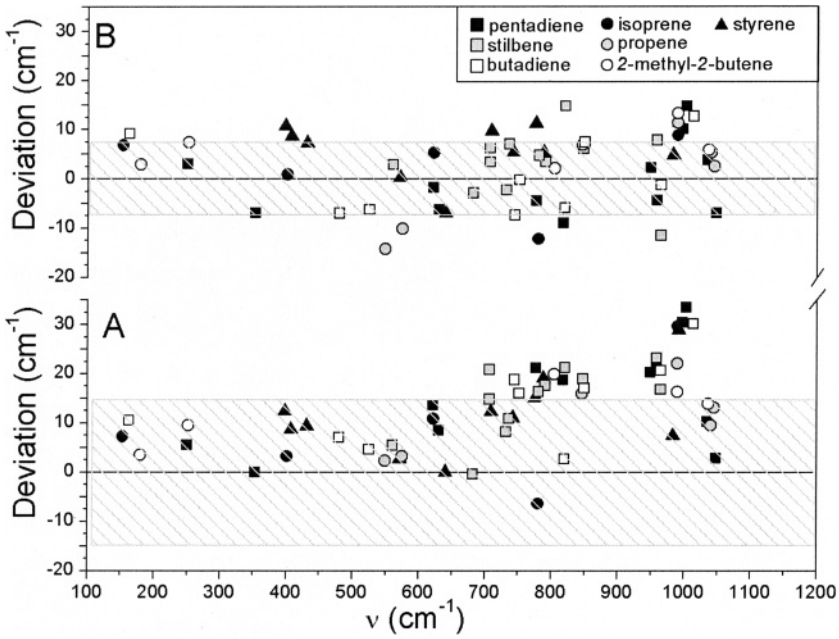

Figure 2. Deviations of the calculated frequencies from the experimental data for the training molecules. Only modes including ethylenic HOOP coordinates with a PED larger than 5% are considered. The HOOP coordinates were scaled with (A) the standard scaling factor for oop coordinates σ_{XYoop} of 0.987 and (B) with the specific scaling factor σ_{HOOP} of 0.90. The shaded areas indicate the respective rms deviations.

structure closely related compounds, we have chosen this geometry for further force field calculations.

For the geometry optimization of PCBE with the protonated (cationic) *ZZZasa* conformation, the starting geometry was taken from the crystal structure of α-CPC,[15] where the tetrapyrrole is embedded in the protein matrix with a carboxylate side chain of Asp87 located near rings B and C. In the present calculations, these interactions were mimicked by placing a chloride counterion between rings B and C, and the covalent linkage to the protein was replaced by a hydrogen link atom. The propionate side chains were modeled with methyl ester groups in order to avoid intramolecular hydrogen-bonding interactions with the pyrrole nitrogens of rings A and D. Since the geometry optimization of $PCBEH^+Cl^-$ was carried out from the tetrapyrrole in vacuo, the resulting geometry with *ZZZasa* configuration is slightly distorted in comparison to the crystallographic structure of the protein-bounded chromophore. The methine bridges of the optimized structure are less twisted than in the protein, indicating that the apoprotein plays an important role in sterically locking the chromophore. Furthermore, the optimized structure of the model compound shows a slight increase of the single/double-bond length alternation at the AB and CD methine bridges accompanied by a closing of the corresponding C═C−C angles, reflecting a decrease of electronic conjugation (Table 2). The optimized structural parameters of the central BC methine bridge are in close agreement with the crystallographic values. Deviations are on the order of 0.01 Å for the C═C and C−C bond lengths and less than 1° for the C═C−C angle.

Optimization of a Force Field Scaling Factor for the Ethylenic CH Out-of-Plane Coordinate. The vibrational spectra of the training set molecules were initially calculated using the standard set of force field scaling factor optimized by Magdo et al.[3] Due to strong coupling with CH_3 rocking (rock) and CH_2 wagging (wag) deformations, the HOOP coordinates are spread among several modes in a wide frequency range between 200 and 1000 cm^{-1}. Furthermore, most of these vibrations are mixed with torsional deformation around the −C═C− and ═C−C− bonds (Tables 1−8, Supporting Information).

Figure 2A displays the deviations between the experimental and the calculated frequencies of all vibrational modes with non-negligible CH oop character. The plot shows that the standard force field scaling factor for the out-of-plane deformation coordinates σ_{XYoop} systematically overestimates the ethylenic HOOP vibrations. These deviations are more pronounced for the high-frequency HOOP, reaching values as high as 33 cm^{-1} such as for pentadiene. It can easily be estimated that no significant improvement will be achieved by employing the scaling factor ($\sigma_{XYoop} = 0.971$) used by Baker,[11] which is only slightly smaller than the one contained in the standard set of scaling factors optimized by Magdo et al.[3] ($\sigma_{XYoop} = 0.987$). Both factors have been optimized for out-of-plane coordinates in general and evidently do not represent a satisfactory correction for the specific ethylenic HOOP coordinates.

Since the CH wag modes of butadiene are mixed with C═C twisting, Magdo et al.[3] tried to correct the overestimation of the calculated CH wag frequencies by using a scaling factor of 0.8681 for the torsional force constant. This procedure is successful for butadiene and for other conjugated noncyclic compounds (e.g., isoprene, pentadiene), in which torsional and HOOP coordinates mix strongly. For molecules such as HMPM, stilbene, or styrene that exhibit much weaker mixing, this correction has no significant effect on the calculated frequencies of the HOOP modes.

A specific scaling factor for the ethylenic HOOP coordinate σ_{HOOP} was, therefore, optimized in this work on the basis of the training molecules propene, 2-methyl-2-butene, butadiene, isoprene, *cis*- and *trans*-pentadiene, *cis*- and *trans*-stilbene, styrene, and HMPM. Monodeuterated propene, butadiene, and HMPM, bideuterated *trans*-stilbene, and trideuterated styrene were also included in the training set, since high-quality vibrational IR and/or Raman spectra are available. After 13 cycles, optimization of σ_{HOOP} converged to 0.900, which is significantly lower than the standard factors σ_{XYoop} of 0.987 and 0.971 determined previously.[3,11] During the optimization procedure, the step size was set to 0.001 with a damping factor of 0.5. A reduction of these optimization parameters only increases the computation time without altering the final result. As shown

TABLE 3: RMS Deviations (in cm^{-1}) of the Calculated Normal-Mode Frequencies[a] for the Training Molecules Using Different Scaling Factors

molecule	no. of modes	RMS $\sigma_{XYoop} = 0.987$	RMS $\sigma_{HOOP} = 0.90$
butadiene	24	16.4	7.3
propene	21	13.1	9.2
isoprene	33	14.9	7.7
2-methyl-2-butene	39	13.9	7.3
cis-1,3 pentadiene	33	16.6	6.0
trans-1,3 pentadiene	33	20.2	8.2
cis-stilbene	72	11.4	5.9
trans-stilbene	72	18.6	7.8
styrene	42	13.8	8.1
HMPM	105	19.2	11.9

[a] Data refer to the modes that include the HOOP coordinate by more than 5% PED.

in Figure 2B, scaling of the force constants with the optimized value $\sigma_{HOOP} = 0.90$ brings the calculated spectra in much closer agreement with the experimental data. The root-mean-square (rms) deviation for all modes with HOOP character was significantly reduced from 16 to 8 cm^{-1} (see Table 3), and the mean of all deviations decreased from 13 to 2 cm^{-1}.

Polyenes. In butadiene, isoprene, *cis*-1,3-pentadiene, as well as in *trans*-1,3-pentadiene, the HOOP coordinates are strongly mixed with torsional coordinates of the C═C and C—C bonds such that in each case several modes exhibit substantial HOOP character (Tables 2−4, Supporting Information). Employing the optimized HOOP scaling factor leads to a substantial decrease of the rms deviations for the calculated frequencies as compared to the experimental data taking from the literature.[17,28] The improved performance also includes the prediction of the frequencies for the respective isotopomers. In addition, the Raman and infrared intensities are well-reproduced with the exception of the ν_{26} mode of the 1,3-pentadiene isomers, which is predicted to exhibit a high Raman intensity in contrast to the experimental findings.

Also for 2-methyl-2-butene, the optimized HOOP scaling factor provides a very good agreement of the experimental spectra reported by Peng et al.[29] and Schrader and Meier[30] (Table 5, Supporting Information). As a specific property of this test molecule, we note an additional strong coupling of the HOOP coordinate with the symmetric and asymmetric CH_3 rocking and the C—$(CH_3)_2$ wagging deformations. The coupling constants calculated for these three coordinates are relatively high (at least 1 order of magnitude) compared to those computed for the remaining coordinates.

A slightly worse performance was observed for propene, in which the ethylenic HOOP coordinate contributes to the potential energy distributions (PED) of at least three vibrational modes: ν_{14}, ν_{15}, and ν_{19} (Table 6, Supporting Information). Among them, ν_{19} exhibits the largest HOOP character (52%). These three modes are undoubtedly assigned to the infrared bands observed at 1045, 990, and 575 cm^{-1},[31] in agreement with a previous study by Takada et al.[32] The modes ν_{15} and ν_{19} show high IR intensity in accordance with the calculations. The optimized scaling factor significantly reduces the deviations of the calculated frequencies for the modes ν_{14} and ν_{15} from 24 to 8 cm^{-1}, whereas the deviation for ν_{19} increases by ca. 6 cm^{-1}. The splitting between the high-frequency (ν_{15}) and low-frequency (ν_{19}) HOOP modes ($\Delta\nu$ = 436.3 cm^{-1}) is thus overestimated in 21 cm^{-1} compared to the experimental data. Modification (by less than 30%) of the coupling constants between the ethylenic HOOP and the CH_3 rock and CH_2 wag coordinates did not improve the theoretical predictions, since ν_{15} and ν_{19} are shifted in the same direction. The same effect is observed for monodeuterated propene. In this respect, deuteration of the ethylenic CH group causes a downshift of ca. 26 cm^{-1} of ν_{19}, which is slightly overestimated by the calculations. Thus, propene is an example for the limitation of the scaling procedure, since a further simultaneous improvement of the calculated frequencies for high and low ethylenic HOOP frequencies cannot be achieved just by scaling the corresponding force fields. However, exclusion of propene from the training set does not significantly affect the result of the optimization of the HOOP scaling factor.

Bridged Conjugated Ring Systems. The vibrational spectra of *trans*- and *cis*-stilbene isomers have been extensively studied previously,[33−36] such that a large set of experimental data is available particularly for *trans*-stilbene (Table 7, Supporting Information). In the experimental spectra of *trans*-stilbene in solution reported by Watanabe,[34] four vibrational bands are detected at 959, 848, 821, and 736 cm^{-1}, which are shifted to slightly higher frequencies in the vibrational spectra of the solid-state sample. In agreement with Arena's results,[33] the first three bands are assigned to vibrational modes with ethylenic HOOP character, since they are strongly shifted to lower wavenumbers (707, 791, and 707 cm^{-1}, respectively) upon deuteration of the ethylene bridge hydrogens. These isotopic shifts are well-reproduced on the basis of the scaling factor σ_{HOOP}. In *cis*-stilbene, the ethylenic HOOP coordinate contributes to five vibrational modes predicted at 952 (ν_{44}), 786 (ν_{50}), 730 (ν_{53}), 679 (ν_{56}), and 564 cm^{-1} (ν_{59}). These modes can be assigned to the experimental bands observed at 965, 781, 732, 698, and 561 cm^{-1} respectively. Among these modes, ν_{44} contains the largest contribution of the ethylenic HOOP coordinates (62% PED). Unlike other training molecules, the ethylenic HOOP coordinates of *cis*-stilbene are mixed with a variety of internal coordinates such as torsions of the ethylenic bridge (ν_{44} and ν_{59}), phenyl CH out-of-plane and puckering deformations (ν_{50}, ν_{56}, and ν_{59}), and C—C═C deformations of the bridge bending (ν_{53}). This strong mixture is a consequence of the non-planar molecular structure of the cis isomer. Our results agree with Arena's assignment for the 781- and 732-cm^{-1} bands,[33] whereas the proposed assignment for medium-intensity Raman band at 965 cm^{-1} as a phenyl ring CH oop mode must be revised. This band disappears in the Raman spectrum of the isotopomer that is doubly deuterated at the ethylene bridge,[30] confirming its ethylenic HOOP character.

It is important to mention that variation of the scaling factor not only induces frequency shifts but also strongly modifies the composition of the vibrational modes. This effect is clearly manifested by modes ν_{50} and ν_{53} of *trans*-stilbene and modes ν_{56} and ν_{59} of *cis*-stilbene, for which the mode composition predicted with the standard scaling factor σ_{XYoop} lacks the contribution of the ethylenic HOOP internal coordinate. Thus, no isotopic shift is calculated for these modes in contrast to the experimental results. Furthermore, the frequencies of the ethylenic HOOP vibrations (ν_{42} and ν_{48} in *trans*-stilbene and ν_{44}, ν_{50}, and ν_{53} in *cis*-stilbene) are overestimated by ca. 20 cm^{-1} with respect to the experimental values. The rms deviation of the frequencies of ethylenic HOOP modes decreases from 24.7 and 14.3 cm^{-1} for *trans*- and *cis*-stilbene to 9.5 and 5.9 cm^{-1}, respectively, when σ_{HOOP} is included in the scaling procedure.

Experimental infrared and Raman spectra of neat styrene and its deuterated derivative have been reported by Condirston and Laposa,[37] and possible vibrational assignments have been suggested on the basis of normal-mode analyses.[35] Due to the strong coupling between the ethylenic HOOP and vinyl wag

TABLE 4: Calculated and Experimental Frequencies (ν, in cm^{-1}) and Intensities for the Modes between 400 and 1000 cm^{-1} of 2,4-Hexadiene Isomers

	exptl			calcd[b]			
mode no.	ν	I_{IR}	I_{Ra}	ν	I_{IR}	I_{Ra}	PED[c] [%]
				(*Z*, *Z*)			
29	950		m	945.5 (972.9)	0	4	[54] HOOP [42] C═C tors
30	926	s		903.0 (903.0)	33	0	[61] C—C stre, [24] CH_3 rock
31	907		m	891.1 (891.1)	0	3	[80] C—C stret
32	770	w		775.2 (804.6)	0	12	[83] HOOP, [11] C═C tors
33	681	s		676.4 (701.2)	52	0	[80] HOOP, [7] C—C tors
34	640		w	630.4 (630.4)	0	5	[54] CCC bend, [23] C—C stre
35	526	m		523.5 (523.6)	16	0	[82] CCC bend
36	470		m	452.5 (460.5)	0	26	[40] HOOP, [52] C—C tors
37	312		w	305.3 (311.3)	0	0	[34] HOOP, [40] C═C tors
rms				9.1 (21.1)			
				(*E*, *E*)			
28	990	s		1001.9 (1023.6)	48	0	[46] HOOP, [46] C═C tors
29				940.9 (966.5)	0	0	[56] HOOP, [42] C═C tors
31	935	m		916.6 (916.6)	28	0	[50] C—C stre, [32] CH_3 rock
32	834		w	825.2 (855.9)	0	14	[80] HOOP
33	750	m		736.5 (763.4)	5	0	[80] HOOP, [12] CH_3 rock
34	554	w		540.7 (540.7)	0	0	[80] CCC bend
35	435		s	426.9 (426.9)	0	13	[55] CCC bend, [29] C—C stre
36	355	w		331.8 (333.2)	0	0	[81] CCC bend
37	334		w	327.7 (331.8)	0	6	[14] HOOP, [50] C═C tors
rms				11.7 (22.8)			
				(*Z*, *E*)			
28		s	w	992.2 (1015.7)	14	1	[51] HOOP, [43] C═C tors
29		s	w	943.6 (970.0)	11	1	[58] HOOP, [40] C═C tors
31		s		917.8 (917.8)	21	1	[25] C—C stre, [40] CH_3 rock
32		w		899.2 (899.2)	11	1	[67] C—C stre, [11] CH_3 rock
33			m	809.5 (839.8)	9	13	[80] HOOP, [7] CH_3 rock
34		s	w	697.5 (723.1)	13	2	[75] HOOP
35		m	m	595.7 (595.7)	5	2	[64] CCC bend, [9] C—C stre
36		m	s	459.6 (459.6)	0	5	[81] CCC bend, [24] C—C stre
37		m	m	427.7 (435.0)	4	10	[39] HOOP, [50] C═C tors
rms				8.3 (23.4)			

[a] Calculated IR (I_{IR}) and Raman intensities (I_{Ra}) are related to the mode of maximum intensity (100). The experimentally determined intensities are classified in terms of strong (s), medium (m), and weak (w) bands. [b] Calculations are based on the specific HOOP scaling factors $\sigma_{HOOP} = 0.90$; data obtained with the standard scaling factor $\sigma_{XYoop} = 0.987$ are given in parentheses. [c] PED, potential energy distribution given in percentage (in brackets). Abbreviations: stre, stretching; bend, bending, tors, torsion.

deformation coordinates, the present calculations predict at least five vibrational modes with non-negligible ethylenic HOOP deformation nature at 1003 cm^{-1} (ν_{24}), 988 cm^{-1} (ν_{25}), 787 cm^{-1} (ν_{31}), 633 cm^{-1} (ν_{34}), and 438 cm^{-1} (ν_{38}) (Table 8, Supporting Information). On the basis of the predicted intensities, ν_{24} and ν_{25} are unambiguously assigned to the strong IR band observed at 992 cm^{-1} and its shoulder at 983 cm^{-1}, respectively. In a similar way, ν_{31} is attributed to the very strong infrared band detected at 776 cm^{-1}. Because ν_{34} and ν_{38} are predicted to exhibit moderate Raman intensity, they are assigned to the Raman bands observed at 640 and 442 cm^{-1}, respectively. Only one pure vinyl wag deformation mode (ν_{29}) is calculated at 915 cm^{-1} with very strong IR intensity, such that it is assigned to the intense IR band observed at 909 cm^{-1}. Deuteration of the ethyl and vinyl hydrogens causes a downshift of these five bands. The absolute frequencies as well as these isotopic shifts are accurately reproduced by the calculations, in which only the ethylenic HOOP coordinate was scaled with σ_{HOOP}, whereas for the C—H oop coordinates of the phenyl and vinyl groups, the standard scaling factor σ_{XYoop} was employed. In this way, the rms deviation of the frequencies of ethylenic HOOP modes of styrene and its deuterated derivative is reduced by a factor of 2.

The vibrational spectra of monomeric and dimeric HMPM have been analyzed in detail previously.[4] Employing the standard scaling factor σ_{XYoop} leads to an overestimation by ca. 20 cm^{-1} of the HOOP mode observed at 888 cm^{-1}. Unlike other training molecules, the HOOP coordinate of HMPM monomer is concentrated in a single mode (ν_{67}) with more than 70% PED. When this internal coordinate is scaled with σ_{HOOP} instead of σ_{XYoop}, the frequency of ν_{67} (878 cm^{-1}) more closely approaches the experimental value. The same effect is observed for ν_{69} of HMPM-CD detected at 759 cm^{-1} and calculated at 751 cm^{-1} with 50% of CD oop character. The isotopic shift of 129 cm^{-1} resulting from H/D substitution at the methine bridge is well reproduced.

From the analysis of the calculated and experimental vibrational spectra of all test molecules, several common features have been noted. First, in conjugated noncyclic systems as well as in styrene, the HOOP coordinate appears to be strongly coupled to wagging deformations of the terminal vinyl groups and to rocking deformations of neighboring methyl groups. This is indicated by the corresponding coupling constants, which are at least 1 order of magnitude higher than other coupling constants. Second, the Raman intensities of the HOOP modes (e.g., ν_{20} of butadiene, ν_{30} and ν_{33} of isoprene, ν_{26} of *cis*- and *trans*-pentadiene, and ν_{34} and ν_{38} of styrene) are generally overestimated. This effect is particularly pronounced for propene where ν_{19} (52% HOOP character) is predicted to be one of the most intense Raman bands, in contrast to the experimental findings. The agreement between calculated and experimental Raman intensities is not improved upon increasing the level of theory, as previously suggested by Stirling (Table 9, Supporting Information).[38] Including diffuse and polarization functions in

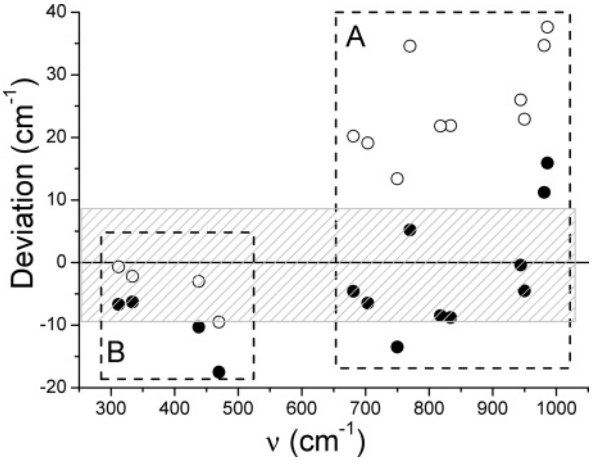

Figure 3. Deviations of the calculated frequencies from the experimental data for hexadiene isomers considering only modes with HOOP character with more than 5% PED. The HOOP coordinates were scaled with the standard scaling factor for oop coordinates σ_{XYoop} of 0.987 (open circles) and with the specific scaling factor σ_{HOOP} of 0.90 (filled circles). The shaded area indicates the rms deviation for the calculations using σ_{HOOP}.

the basis set strongly affects the Raman activities of low-frequency vibrational modes but does not lead to a uniform decrease of the calculated Raman intensities. This failure is not restricted to DFT but also noted for the MP2/6-31++g** calculations. Interestingly, the calculated Raman intensities of the HOOP modes of the remaining training molecules, stilbene, HMPM, and 2-methyl-2-butene, are consistent with the respective experimental spectra.

Test and Target Molecules. *Hexadiene.* The HOOP coordinates contribute to the PEDs of five modes in a wide frequency range between 1000 and 300 cm^{-1}, among which only two involve more than 80% HOOP character. For the three hexadiene conformers, the frequencies of these two modes are calculated at between 700 and 750 cm^{-1} and 800−750 cm^{-1}, which agree very well with the experimental data for the (*Z*,*Z*) (681 and 770 cm^{-1}), (*Z*,*E*) (704 and 818 cm^{-1}), and (*E*,*E*) (750 and 834 cm^{-1}) conformers (Table 4).[39]

The HOOP modes of the three isomers can be sorted into two main groups according to the frequencies above 600 cm^{-1} (group A) and below 600 cm^{-1} (group B). The standard scaling factor σ_{XYoop} strongly overestimates the frequencies of group A with deviations higher than 13 cm^{-1}, whereas it slightly underestimates the frequencies of group B with a maximum deviation of −9 cm^{-1} (Figure 3). Although scaling with the scaling factor σ_{HOOP} is only successful at the high-frequency range, there is a significant reduction of the rms deviation from ca. 22 to 9 cm^{-1}. All hexadiene isomers studied in this work display an overestimation of the calculated Raman activities of the HOOP modes as already discussed for noncyclic conjugated training molecules (vide supra). The modes ν_{32} of the (*Z*,*Z*) and (*E*,*E*) hexadiene isomers are calculated with considerable Raman intensities in contradiction to the experimental spectrum. In the case of the (*Z*,*E*) isomer, the Raman intensity pattern predicted between 900 and 400 cm^{-1} strongly deviates from the experimental spectra.[39] Here, two relatively strong bands are predicted at 810 and 428 cm^{-1}, and a much lower intensity is calculated for the mode at 460 cm^{-1}. The experimental spectrum displays one strong band at 465 cm^{-1} and two medium-intensity bands at 818 and 438 cm^{-1}.

Phycocyanobilin Dimethylester. The experimental RR spectra of PCBE and the PCB chromophore embedded in the protein matrix of α-CPC protein[13,40] have been compared with the

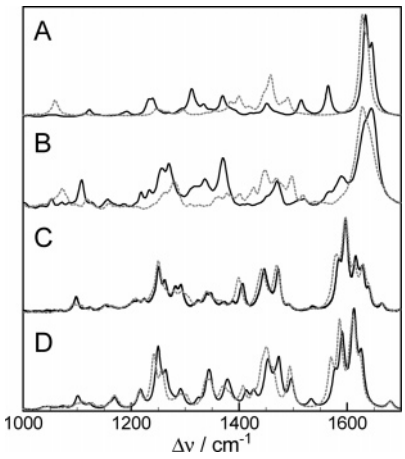

Figure 4. Calculated Raman spectrum of (A) PCBEH$^+$Cl$^-$ in the *ZZZasa* configuration and (D) of the PCBE dimer in the *ZZZsss* configuration in the frequency range from 1000 to 1700 cm^{-1}. Traces (B) and (C) show the experimental RR of α-CPC and solid PCBE, respectively. The gray dotted lines refer to the chromophores deuterated at the pyrrole nitrogens.

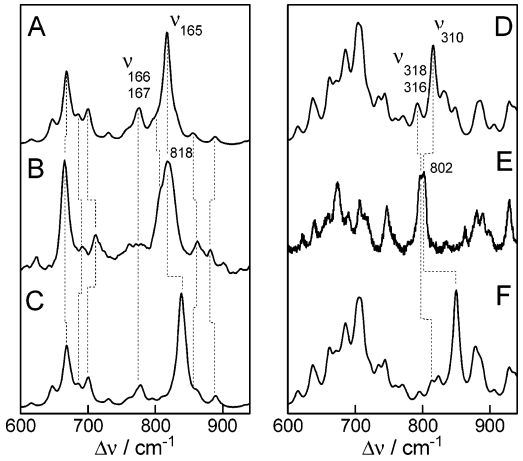

Figure 5. Left column: calculated low-frequency Raman spectra of PCBEH$^+$Cl$^-$ in the *ZZZasa* configuration using (C) the standard scaling factor for oop coordinates σ_{XYoop} of 0.987 and (A) the specific scaling factor σ_{HOOP} of 0.90. The experimental RR spectrum of α-CPC is shown in (B). Right column: calculated low-frequency Raman spectra of the PCBE dimer in the *ZZZsss* configuration using (F) the standard scaling factor for oop coordinates σ_{XYoop} of 0.987 and (D) the specific scaling factor σ_{HOOP} of 0.90. The experimental RR spectrum of PCBE is shown in (E).

calculated Raman spectra of PCBE with *ZZZsss* configuration and the Raman spectra of PCBEH$^+$Cl$^-$ with *ZZZasa* configuration, respectively. In the frequency range between 1000 and 1700 cm^{-1}, which is not affected by variation of the scaling factor for HOOP coordinates, we note a very good agreement for both tetrapyrroles in H_2O and D_2O (Figure 4). Note that both the frequencies and the intensities are well-reproduced even though the experimental spectra have been measured under preresonance conditions. Below 1000 cm^{-1}, however, the proper scaling of the HOOP coordinates has a pronounced effect on the calculated spectra and provides an improved description of the experimental spectra (Figure 5).

DFT calculations of dimeric PCBE (*ZZZsss* configuration) using the standard set of force field scaling factors predict a prominent Raman band at 849 cm^{-1} which, as well as the much weaker bands at 813 and 877 cm^{-1}, exhibits significant contributions of the HOOP coordinates (ca. 50%). The experimental Raman spectrum of PCBE shows a distinct albeit weak

TABLE 5: Calculated and Experimental Frequencies (ν, in cm^{-1}) and Intensities for the Selected Modes Between ca. 800 and 900 cm^{-1} of Protonated Phycocyanobilin Dimethylester in the *ZZZasa* Configuration and Dimeric Phycocyanobilin Dimethylester in the *ZZZsss* Configuration[a]

	exptl		calcd			
mode no.	ν	I_{RR}	ν	I_{IR}	I_{Ra}	PED[b] [%]
			CPC (*ZZZasa*)			
158	882	w	874.0 (907.1)	20 (6)	2 (0)	[69] HOOP (BC), [11] C═C tors (BC), [7] C—C tors (BC)
159			866.0 (866.6)	101 (128)	0 (0)	[11] C—O stre, [14] C—C stre
160	862	w	860.3 (863.4)	6 (10)	1 (2)	[26] C—C stre, [16] ethyl rock
161			855.8 (859.1)	90 (129)	2 (1)	[6] C—C stre
162			832.1 (843.8)	152 (118)	3 (9)	[13] HOOP (AB), [5] HOOP (AB), [36] NH oop (B), [21] NH oop (C)
163			825.8 (826.2)	27 (8)	2 (2)	[6] HOOP (CD), [16] CH_2 rock
164	825	sh	823.6 (823.6)	24 (22)	0 (0)	[28] C—O stre, [7] C—C stre
165	818	m	817.5 (838.0)	27 (47)	29 (30)	[35] HOOP (BC), [14] HOOP (AB), [7] C═C tors (BC)
166	806	sh	811.7 (809.5)	16 (3)	4 (1)	[22] C—C stre, [6] HOOP (CD), [6] NH oop (B)
167			803.2 (814.)	27 (39)	3 (1)	[24] HOOP (AB), [6] HOOP (CD), [14] NH oop (C), [14] NH oop (B)
			PCBE Dimer (*ZZZsss*)			
303			851.2 (850.4)	0	2	[16] CH oop (BC), [24] ethylidene CH oop (A)
304			851.1 (850.3)	27	0	[16] HOOP (BC), [29] ethylidene CH oop (A)
305			848.1 (876.6)	15	0	[50] HOOP (BC)
306	835	w	848.0 (876.5)	0	4	[50] HOOP (BC)
307			834.8 (834.8)	26	0	[24] CC stre
308			834.7 (834.2)	0	3	[24] CC stre
309			822.9 (848.3)	18	0	[60] HOOP (CD)
310	802	m	822.1 (848.5)	0	20	[62] HOOP (CD)
316			793.1	0	2	[16] HOOP (AB)
317			790.5 (813.2)	59	0	[46] HOOP (AB)
318	781	m	790.3 (813.2)	0	3	[36] HOOP (AB)

[a] Calculations are based on the specific HOOP scaling factors $\sigma_{HOOP} = 0.90$; data obtained with the standard scaling factor $\sigma_{XYoop} = 0.987$ are given in parentheses. Calculated IR (I_{IR}) and Raman intensities (I_{Ra}) are related to the mode of maximum intensity (100). The experimentally determined RR intensities (I_{RR}) are classified in terms of medium (m) and weak (w) bands and shoulders (sh). [b] PED, potential energy distribution given in percentage (in brackets). Abbreviations: stre, stretching; bend, bending, tors, torsion. The individual rings of the tetrapyrroles are denoted by the letters A, B, C, and D, thereby also defining the respective methine bridges (AB, BC, and CD) (Figure 1).

band at 802 cm^{-1}, which thus is attributed to the mode at 849 cm^{-1} despite the ca. 50-cm^{-1} deviation.

Upon introducing the HOOP scaling factor σ_{HOOP}, frequencies of the modes between 900 and 780 cm^{-1} are substantially altered (Table 5). The 849 cm^{-1} mode including the HOOP mode of the C—D methine bridge is now calculated at 822 cm^{-1} (ν_{310}) and predicted to exhibit a considerable Raman intensity such that the assignment to the experimental band at 802 cm^{-1} is straightforward. Furthermore, in addition, the low-frequency shoulder at 781 cm^{-1} in the experimental spectrum is now much better matched by the calculated Raman-active modes ν_{318} (790 cm^{-1}) and ν_{316} (793 cm^{-1}) that include the HOOP coordinate of the A—B methine bridge. Thus, the deviations from the experimental frequencies are substantially reduced.

Protein-Bound Phycocyanobilin. For the protonated *ZZZasa* PCB in α-CPC, previous DFT calculations done using the standard set of scaling factors have predicted several vibrational modes with non-negligible methine bridge HOOP character.[40] Only for two of these modes has a significant Raman intensity been predicted, and their frequencies have been calculated to be higher by more than 20 cm^{-1} than for the experimental band at 818 cm^{-1} (Figure 5C). Including σ_{HOOP} also causes alterations of the PEDs for the normal modes in this region such that four modes instead of five possess appreciable contributions from the methine bridge HOOP coordinates. Now, the frequency deviations are drastically reduced (Table 5). Specifically, the mode ν_{162} (HOOP of C—D methine bridge) for which the highest Raman intensity is calculated agrees very well with the prominent experimental band at 818 cm^{-1}. The modes including HOOP coordinates of the methine bridges A—B and B—C character (ν_{158}, ν_{162}, and ν_{167}) are calculated with low Raman intensities such that an unambiguous assignment is not possible.

The Pr State of Phytochrome. The recent crystal structure analysis of the chromophore-binding fragment of phytochrome DrBphP from *Deinococcus radiodurans* has unambiguously revealed a *ZZZssa* configuration of the chromophore in the parent state Pr,[41] which has been further shown to be protonated in neutral aqueous solution (unpublished results). However, there are indications that this configuration is only true for biliverdin-binding phytochromes, whereas, possibly due to the different binding site in the chromophore pocket, for PCB- and phytochromobilin-binding phytochromes such as phyA from plants the Pr chromophore appear to adopt a protonated (cationic) *ZZZasa* configuration.[6] This conclusion has been derived from the analysis of the RR spectra in the spectral region between 1200 and 1700 cm^{-1}. Whereas in this region the calculations agree very well with the experimental data, there are significant discrepancies in the region below 1000 cm^{-1}. Calculations that are based on the extended set of scaling factors including σ_{HOOP} improve the description of the RR spectra between 600 and 900 cm^{-1} (Figure 6), although the agreement is not as good as in the case of α-CPC. Such a discrepancy is not observed for the RR spectrum of the Pr state of the phyA adduct assembled with PCB, which is deuterated at the C—D methine bridge. For this isotopomer, the C—D oop coordinate contributes to three closely spaced modes of medium Raman intensity at 602, 601, and 598 cm^{-1}, which together lead to the most intense band in the calculated spectrum below 1000 cm^{-1}. The frequency of the resultant peak exactly coincides with the RR band observed at 601 cm^{-1}. This band is also the most intense band in the experimental RR spectrum in this region, although, due to the poor signal-to-noise ratio, further bands cannot be identified. This agreement as well as the good performance of the calculations for the PCBE dimer and α-CPC rules out that an inadequate scaling factor for the HOOP coordinate is the origin for the insufficient reproduction of the experimental RR spectrum of Pr spectra below 1000 cm^{-1}. Instead, these deviations evidently reflect the limitations of in vacuo calcula-

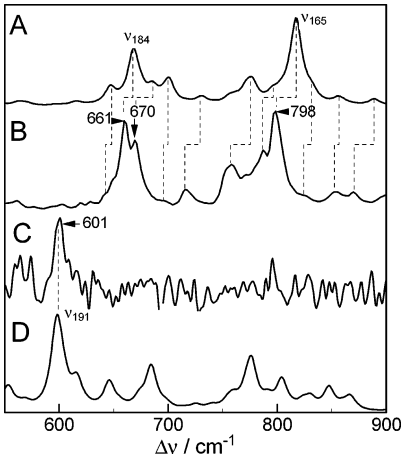

Figure 6. Calculated low-frequency Raman spectrum of (A) $PCBEH^{+}$-Cl^{-} in the *ZZZasa* and (D) its isotopomer deuterated at the C-15 carbon. The experimental RR spectra of recombinant phytochrome (phyA) adducts in the P_r state including the nonlabeled and the C-15 deuterated PCB chromophore are shown in (B) and (C), respectively.

tions for the protein-bound chromophore in phytochrome. It may be that specific protein−chromophore interactions in the Pr state cause a tetrapyrrole geometry that deviates in details from the "ideal" *ZZZasa* configuration as optimized by in vacuo calculations. In contrast, the photochemically inert chromophore in α-CPC seems to adopt a relaxed structure as judged from the good agreement between the experimental and calculated spectra.

Conclusions

1. DFT(B3LYP) calculations significantly overestimate the frequencies of modes dominated by ethylenic HOOP coordinates. This deficiency cannot be adequately compensated by using scaling factors suitable for other *X*−*Y* oop coordinates (0.971−0.987).

2. On the basis of a set of training molecules, a specific scaling factor for the ethylenic HOOP coordinate (0.900) has been optimized that leads to a substantial improvement of the reproduction of the experimental frequencies for the HOOP-containing modes.

3. Prediction of Raman intensities for these modes, however, is still associated with a considerable error, which in most cases is reflected by an overestimation of the Raman activities. No significant improvement is achieved by using larger basis sets for DFT or MP2 calculations.

4. Despite these drawbacks, the inclusion of the specific HOOP scaling factor in the set of global scaling factors also provides a good description for the experimental Raman spectra of test molecules as large as tetrapyrrole dimers and the protein-bound PCB in α-CPC.

5. The larger deviations for the protein-bound tetrapyrrole in phytochrome are attributed to the effect of the protein environment which is not considered by the in vacuo calculations. To extract structural information also beyond the level of methine bridge configuration and conformation from the low-frequency RR spectra, hybrid methods are required that also include the protein environment.

Acknowledgment. The work was supported by the Deutsche Forschungsgemeinschaft (Sfb498). Recombinant phytochrome including PCB and its C-15 deuterated isotopomer was provided by Wolfgang Gärtner, Mülheim.

Supporting Information Available: Tables of structural data of hexadiene isomers, calculated and experimental frequencies and IR and Raman intensities of butadiene, isoprene, pentadiene, 2-methyl-2-butene, propene, stilbene, and styrene isomers and isotopomers. This material is available free of charge via the Internet at http://pubs.acs.org.

References and Notes

(1) Rauhut, G.; Pulay, P. *J. Phys. Chem.* **1995**, *99*, 3093.
(2) Arenas, J. F.; Otero, J. C.; Sanchez Galvez, A.; Soto, J. *J. Mol. Struct.* **1996**, *385*, 49.
(3) Magdo, I.; Nemeth, K.; Mark, F.; Hildebrandt, P.; Schaffner, K. *J. Phys. Chem. A* **1999**, *103*, 289.
(4) Mroginski, M. A.; Nemeth, K.; Bauschlicher, T.; Klotzbucher, W.; Goddard, R.; Heinemann, O.; Hildebrandt, P.; Mark, F. *J. Phys. Chem. A* **2005**, *109*, 2139.
(5) Kneip, C.; Hildebrandt, P.; Schlamann, W.; Braslavsky, S. E.; Mark, F.; Schaffner, K. *Biochemistry* **1999**, *38*, 15185.
(6) Mroginski, M. A.; Murgida, D. H.; von Stetten, D.; Kneip, C.; Mark, F.; Hildebrandt, P. *J. Am. Chem. Soc.* **2004**, *126*, 16734.
(7) Borucki, B.; von Stetten, D.; Seibeck, S.; Lamparter, T.; Michael, N.; Mroginski, M. A.; Otto, H.; Murgida, D. H.; Heyn, M. P.; Hildebrandt, P. *J. Biol. Chem.* **2005**, *280*, 34358.
(8) Kneip, C.; Mozley, D.; Hildebrandt, P.; Gartner, W.; Braslavsky, S. E.; Schaffner, K. *FEBS Lett.* **1997**, *414*, 23.
(9) Becke, A. D. *J. Chem. Phys.* **1993**, *98*, 5648.
(10) Ditchfield, R.; Hehre, W. J.; Pople, J. A. *J. Chem. Phys.* **1972**, *56*, 2257.
(11) Baker, J.; Jarzecki, A. A.; Pulay, P. *J. Phys. Chem. A* **1998**, *102*, 1412.
(12) Frisch, M. J.; Trucks, G. W.; Schlegel, H. B.; Scuseria, G. E.; Robb, M. A.; Cheeseman, J. R.; Montgomery, J. A., Jr.; Vreven, T.; Kudin, K. N.; Burant, J. C.; Millam, J. M.; Iyengar, S. S.; Tomasi, J.; Barone, V.; Mennucci, B.; Cossi, M.; Scalmani, G.; Rega, N.; Petersson, G. A.; Nakatsuji, H.; Hada, M.; Ehara, M.; Toyota, K.; Fukuda, R.; Hasegawa, J.; Ishida, M.; Nakajima, T.; Honda, Y.; Kitao, O.; Nakai, H.; Klene, M.; Li, X.; Knox, J. E.; Hratchian, H. P.; Cross, J. B.; Bakken, V.; Adamo, C.; Jaramillo, J.; Gomperts, R.; Stratmann, R. E.; Yazyev, O.; Austin, A. J.; Cammi, R.; Pomelli, C.; Ochterski, J. W.; Ayala, P. Y.; Morokuma, K.; Voth, G. A.; Salvador, P.; Dannenberg, J. J.; Zakrzewski, V. G.; Dapprich, S.; Daniels, A. D.; Strain, M. C.; Farkas, O.; Malick, D. K.; Rabuck, A. D.; Raghavachari, K.; Foresman, J. B.; Ortiz, J. V.; Cui, Q.; Baboul, A. G.; Clifford, S.; Cioslowski, J.; Stefanov, B. B.; Liu, G.; Liashenko, A.; Piskorz, P.; Komaromi, I.; Martin, R. L.; Fox, D. J.; Keith, T.; Al-Laham, M. A.; Peng, C. Y.; Nanayakkara, A.; Challacombe, M.; Gill, P. M. W.; Johnson, B.; Chen, W.; Wong, M. W.; Gonzalez, C.; Pople, J. A. *Gaussian 03*; Gaussian, Inc.: Wallingford, CT, 2004.
(13) Kneip, C.; Parbel, A.; Foerstendorf, H.; Scheer, H.; Siebert, F.; Hildebrandt, P. *J. Raman Spectrosc.* **1998**, *29*, 939.
(14) Mohamed, T. A.; Aly, M. M. A. *J. Raman Spectrosc.* **2004**, *35*, 869.
(15) Duerring, M.; Huber, R.; Bode, W. *J. Mol. Biol.* **1990**, *211*, 633.
(16) Takahashi, H.; Kuroyanagi, K.; Yamada, O.; Kaneko, N. *Chem. Phys. Lett.* **2003**, *94*, 38.
(17) Compton, D. A. C.; George, W. O.; Maddams, W. F. *J. Chem. Soc., Perkin Trans. 2* **1976**, 1666.
(18) Traetteberg, M.; Paulen, G.; Cyvin, S. J.; Panchenko, Y. N.; Mochalov, V. I. *J. Mol. Struct.* **1984**, *116*, 141.
(19) Kuchitsu, K.; Fukuyama, T.; Morino, Y. *J. Mol. Struct.* **1968**, *1*, 463.
(20) Lide, D. R.; Christensen, D. *J. Chem. Phys.* **1961**, *35*, 1374.
(21) Hsu, S. L.; Flygare, W. H. *J. Chem. Phys.* **1970**, *52*, 1053.
(22) Traetteberg, M.; Frantsen, E. B. *J. Mol. Struct.* **1975**, *26*, 69.
(23) Traetteberg, M.; Frantsen, E. B.; Mijlhoff, F. C.; Hoekstra, A. *J. Mol. Struct.* **1975**, *26*, 57.
(24) Yasuda, N.; Uekusa, H.; Ohashi, Y. *Acta Crystallogr., Sect. E* **2001**, *57*, O1189−O1190.
(25) Knipp, B.; Müller, M.; Metzler-Nolte, N.; Balaban, T. S.; Braslavsky, S. E.; Schaffner, K. *Helv. Chim. Acta* **1998**, *81*, 881.
(26) Kratky, C.; Falk, H.; Grubmayr, K. *Monatsh. Chem.* **1985**, *116*, 745.
(27) Sheldrick, W. S. *Isr. J. Chem.* **1983**, *23*, 155.
(28) Compton, D. A. C.; George, W. O.; Maddams, W. F. *J. Chem. Soc., Perkin Trans. 2* **1977**, 1311.
(29) Peng, J. P.; Minacamilde, N.; Manzanares, C. *Vib. Spectrosc.* **1995**, *8*, 319.
(30) Schrader, B.; Meier, W. *DMS Raman/IR Atlas of Organic Compounds*; Verlag Chemie GmbH: Weinheim, 1975.
(31) Silvi, B.; Labarbe, P.; Perchard, J. P. *Spectrochim. Acta, Part A* **1973**, *A 29*, 263.

(32) Takada, T.; Dupuis, M. *J. Am. Chem. Soc.* **1983**, *105*, 1713.
(33) Arenas, J. F.; Tocon, I. L.; Otero, J. C.; Marcos, J. I. *J. Phys. Chem.* **1995**, *99*, 11392.
(34) Watanabe, H.; Okamoto, Y.; Furuya, K.; Sakamoto, A.; Tasumi, M. *J. Phys. Chem. A* **2002**, *106*, 3318.
(35) Choi, C. H.; Kertesz, M. *J. Phys. Chem. A* **1997**, *101*, 3823.
(36) Meic, Z.; Gusten, H. *Spectrochim. Acta, Part A* **1978**, *34*, 101.
(37) Condirston, D. A.; Laposa, J. D. *J. Mol. Spectrosc.* **1976**, *63*, 466.
(38) Stirling, A. *J. Chem. Phys.* **1996**, *104*, 1254.
(39) Aly, M. M. A.; Baron, M. H.; Romain, F.; Revault, M. *Spectrochim. Acta* **1984**, *40*, 1037.
(40) Kneip, C.; Hildebrandt, P.; Nemeth, K.; Mark, F.; Schaffner, K. *Chem. Phys. Lett.* **1999**, *311*, 479.
(41) Wagner, J. R.; Brunzelle, J. S.; Forest, K. T.; Vierstra, R. D. *Nature (London)* **2005**, *438*, 325.